

The Stellar Content of Obscured Galactic Giant H II Regions: II. W42

R. D. Blum¹

Cerro Tololo Interamerican Observatory, Casilla 603, La Serena, Chile
rblum@noao.edu

P. S. Conti

JILA, University of Colorado
Campus Box 440, Boulder, CO, 80309
pconti@jila.colorado.edu

A. Damineli

IAG-USP, Av. Miguel Stefano 4200, 04301-904, São Paulo, Brazil
damineli@iagusp.usp.br

ABSTRACT

We present near infrared J , H , and K images and K –band spectroscopy in the giant H II region W42. A massive star cluster is revealed; the color–color plot and K –band spectroscopic morphology of two of the brighter objects suggest the presence of young stellar objects. The spectrum of the bright central star is similar to unobscured stars with MK spectral types of O5–O6.5. If this star is on the zero age main sequence, then the derived spectrophotometric distance is considerably smaller than previous estimates. The Lyman continuum luminosity of the cluster is a few times that of the Trapezium. The slope of the K –band luminosity function is similar to that for the Trapezium cluster and significantly steeper than that for the massive star cluster in M17 or the Arches cluster near the Galactic center.

Subject headings: H II regions — infrared: stars — stars: early–type — stars: fundamental parameters — stars: formation

1. INTRODUCTION

In this paper we continue the exploration of the stellar content of obscured Galactic giant H II regions begun by Blum et al. (1999, hereafter Paper I). J , H , and K images are used to

¹Visiting Astronomer, Cerro Tololo Interamerican Observatory, National Optical Astronomy Observatories, which is operated by Associated Universities for Research in Astronomy, Inc., under cooperative agreement with the National Science Foundation

make a broad assessment of the stellar content of obscured star forming regions in the Milky Way. Infrared spectroscopy follows, providing details of the brightest cluster members which can be used to make distance, mass, and luminosity estimates. The spectra are placed in proper context by comparison to new infrared spectral classification systems for massive stars (Hanson et al. 1996; Blum et al. 1997; Figer et al. 1997; Hanson et al. 1998). The known hot star content of the Galaxy is rapidly expanding on the strength of the sophisticated infrared detector gains of the last 10 years. Hanson et al. (1997) have recently published a very detailed account of the most massive stars in the (relatively) nearby giant H II region M17. The present project (Paper I, this work, and future work) seeks to provide a large sample of massive star clusters with which to study the young and massive stellar content in the Galaxy. This sample builds on the detailed visual studies of the Galactic OB associations (Massey et al. 1995) and provides a bridge to studies of young stellar objects in star forming regions. Finally, the investigation of a large sample of clusters in Galactic giant H II regions will be important in understanding the massive star clusters in the Galactic center (Cotera et al. 1996; Figer et al. 1999a,b) which may have formed under different conditions than are typical in the disk of our Galaxy (Morris & Serabyn 1996).

W42 is located in the fourth Galactic quadrant at $l, b = 25.4^\circ, 0.2^\circ$. Lester et al. (1985) determined W42 to be at the “near” kinematic distance (3.7 kpc for $R_\odot = 8$ kpc) and hence somewhat less luminous than earlier estimates (Smith et al. 1978). In this series of papers we shall follow a suggestion of Dr. Robert Kennicutt (private communication) that “giant” means that more than 10^{50} Lyman continuum (= Lyc) photons are inferred to be emitted per second from the H II region. This is about ten times the luminosity of the Orion nebula and roughly the number emitted from the hottest *single* O3-type star. As these stars are not found in isolation, there is an implication that a “giant” H II region contains some minimum of *multiple* O-type stars. In light of our new distance estimate (see §4), W42 probably falls below this limit being perhaps a few times more luminous than the Trapezium in Orion. Our target list was originally based on eleven of the most luminous giant H II regions from the study of (Smith et al. 1978) who tabulated their Lyc output derived from radio continuum measurements and kinematic distance estimates. W42 is not seen in visual images, and we estimate a foreground extinction of $A_V = 10$ mag (see below).

2. OBSERVATIONS AND DATA REDUCTION

J ($\lambda \sim 1.3 \mu\text{m}$, $\Delta\lambda \sim 0.3 \mu\text{m}$), H ($\lambda \sim 1.6 \mu\text{m}$, $\Delta\lambda \sim 0.3 \mu\text{m}$), and K ($\lambda \sim 2.2 \mu\text{m}$, $\Delta\lambda \sim 0.4 \mu\text{m}$) images of W42 were obtained on the nights of 29 August 1998 and 01, 02 May 1999 with the f/14 tip–tilt system on the Cerro Tololo Interamerican Observatory (CTIO) 4m Blanco telescope using the two facility imagers CIRIM (1998 data) and OSIRIS, the Ohio State InfraRed Imager/Spectrometer² (1999 data). Spectroscopic data were obtained on the night of 02

²OSIRIS is a collaborative project between the Ohio State University and CTIO. OSIRIS was developed through NSF grants AST 9016112 and AST 9218449.

May 1999 using the f/14 tip–tilt system at the Blanco telescope with OSIRIS. CIRIM and OSIRIS are described in the instrument manuals found on the CTIO web pages (www.ctio.noao.edu). For OSIRIS, see also DePoy et al. (1993). The tip–tilt system is described by Pérez & Elston (1998). The tip–tilt system uses three piezo–electric actuators to move the secondary mirror at high frequency in a computer controlled feed–back loop which corrects the natural image centroid motion. OSIRIS employs 0.16" pixels and CIRIM 0.21" pixels.

All basic data reduction was accomplished using IRAF³. Each image/spectrum was flat–fielded using dome flats and then sky subtracted using a median combined image of five to six frames. For W42 itself, independent sky frames were obtained five to ten arcminutes south of the cluster. Standard stars used the median combination of the data for sky.

2.1. Images

The OSIRIS 1999 May images were obtained under photometric conditions and in $\sim 0.5''$ to $0.6''$ FWHM seeing (with the tip–tilt correction). Total exposure times were 270 s, 135 s, and 135 s at J , H , and K , respectively. The individual J , H , and K frames were shifted and combined (Figure 1), and these combined frames have point sources with FWHM of $\sim 0.6''$, $0.7''$, and $0.6''$ at J , H , and K , respectively. DoPHOT (Schecter et al. 1993) photometry was performed on the combined images. The flux calibration was accomplished using standards 9170 and 9172 from Persson et al. (1998) which are on the Las Campanas Observatory standard system (LCO). The LCO standards are essentially on the CIT/CTIO system (Elias et al. 1982), though color transformations exist between the two systems for redder stars. The standards were taken just before the W42 data and within 0.16 airmass of the airmass for W42; no corrections were applied for these small differences in airmass. Aperture corrections using 11 pixel radius apertures were used to put the instrumental magnitudes on a flux scale.

Stars brighter than about 10th magnitude are expected to be a few percent non-linear on the OSIRIS images. We have included the 1998 CIRIM data for such stars since the count levels for the CIRIM images were in the fully linear regime (no linearity correction needed). The zero point to the CIRIM photometry was determined by comparing the instrumental magnitudes of stars in common to the OSIRIS and CIRIM images. The CIRIM J –band photometry includes a color correction term in order to make a transformation on to the CIT/CTIO system (PAPER I). The OSIRIS data was placed on the CIT/CTIO system by making small corrections (< 10 %) to the J , H and K magnitudes based on linear fits to the magnitude differences as a function of color for stars in common to the CIRIM and OSIRIS images.

Uncertainties for the final JHK magnitudes include the formal DoPHOT error added in quadrature to the error in the mean of the photometric standards (including the transformation to

³IRAF is distributed by the National Optical Astronomy Observatories.

OSIRIS magnitudes for the CIRIM data), and the error in aperture corrections used in transforming from the DoPHOT photometry to OSIRIS magnitudes. The latter errors dominate and were derived from the scatter in the measurements of four to seven relatively uncrowded stars on the mosaic frames. The sum (in quadrature) of the aperture correction and standard star uncertainties is ± 0.018 , ± 0.023 , ± 0.019 mag in J , H , and K , respectively. The DoPHOT errors ranged from approximately ± 0.01 mag to an arbitrary cut-off of 0.2 mag (stars with larger errors were excluded from further analysis).

The flat-field illumination was not uniform. A smooth gradient with full range of about 10% was present. Corrections for this gradient were made based on observations of a standard star taken over a 49 position grid covering the array.

2.2. Spectra

The spectra of three of the brightest four stars in the center of W42 were obtained with a $0.48''$ wide slit (oriented EW) in $\lesssim 0.7''$ FWHM seeing and divided by the spectrum of HR 6813 (A1V) to remove telluric absorption features. Br γ absorption in HR 6813 was removed by eye by drawing a line across it between two continuum points. One dimensional spectra were obtained by extracting and summing the flux in a ± 2 pixel aperture ($0.64''$ wide). The extractions include background subtraction from apertures centered $\lesssim 1.0''$ on either side of the object.

The wavelength calibration was accomplished by measuring the positions of bright OH $^-$ lines from the K -band sky spectrum (Olivia & Origlia 1992). Lines are identified by their relative differences between one and another. The measured dispersion is $0.0003683 \mu\text{m pix}^{-1}$. The spectral resolution at $2.2 \mu\text{m}$ is $\lambda/\Delta\lambda \approx 3000$.

3. RESULTS

A spectacular stellar cluster is revealed at the heart of W42 in our near infrared images (Figure 1 and Figure 2). Apparently, the cluster has just emerged from the edge of the molecular cloud from which it formed. This is confirmed below through K -band spectroscopy which shows that the central massive star has largely cleared away its birth cocoon, but two of the next brightest stars have not. Lester et al. (1985) observed W42 in the mid and far infrared. Their analysis revealed two distinct sites of star formation toward W42. One, G25.4SE is located at 3.7 kpc from the sun (accounting for a sun to Galactic center distance of 8 kpc), while the other, G25.4NW is probably located at about 9.6 kpc. Lester et al. found a $10 \mu\text{m}$ unresolved source located at RA (2000) = $18^{\text{h}} 38^{\text{m}} 15^{\text{s}}.2$, Dec (2000) = $-06^{\circ} 47' 50''$ which is coincident with G25.4SE. This mid IR source is associated with the stellar cluster we have observed. Comparison of the position of the bright foreground star in the SE corner of our K -band image to the same star on the image from

the Digitized Sky Survey (DSS)⁴ results in a position for the (K –band) bright central star in the cluster (W42 #1; see §3.2) of RA (2000) = $18^{\text{h}} 38^{\text{m}} 15^{\text{s}}.3$, Dec (2000) = $-06^{\circ} 47' 58''$.

3.1. Images

The $H - K$ color–magnitude diagram (CMD) for the region toward W42 is shown in Figure 3. A cluster sequence is evident at $0.6 \lesssim H - K \lesssim 1.5$ along with stars with much redder colors and a probable foreground sequence. The $J - H$ vs. $H - K$ color–color diagram is presented in Figure 4. As expected from the morphology and range of colors in Figure 2, the strong effects of differential reddening can be seen in the color–color diagram. Typical reddening lines are shown for M giants (Frogel et al. 1978) and early O stars (Koornneef 1983a). The latter color was transformed as described in §3.1.3. The cluster stars defined below in §3.1.1 and shown as *open circles* in Figure 4 may have a slight unexplained systematic offset relative to the reddening line for normal O stars. This possible offset will not affect the conclusions in this paper regarding the cluster stars. The relationship for the intrinsic colors of classical T Tauri stars (pre–main sequence stars) (Meyer et al. 1997) is also shown for reference. The adopted reddening law is from Mathis (1990).

3.1.1. The Central Cluster

By separating the stars in Figure 3 based on radial position, we can better define the central cluster relative to the surrounding field. In Figure 5, we plot the radial surface density of stars centered on the position of the bright central star, W42 #1 (§3.2). We also plot the radial surface density for stars with $K \leq 14$ mag, for which the number counts are more nearly complete (see below). The surface density becomes approximately uniform at a radius of $R \sim 30''$, continuing up to $50''$. It then begins to fall rapidly at the edge of the array (*dashed vertical line*) as expected due to the rectangular shape of the field. Taking these radii as representative, we divide the CMD into regions with $0'' \leq R < 30''$, $30'' \leq R < 50''$, and $R > 50''$, as shown in Figure 6. These represent the central cluster, a background annulus, and the region of the array where edge effects are important to the radial number counts.

The range of color and brightness in Figure 6 overlaps for stars in the cluster and background regions. A distinct blue sequence can be seen in the $0'' \leq R < 30''$ cluster CMD which appears to merge smoothly with other stars in the $30'' \leq R < 50''$ CMD. Clearly the cluster can not be

⁴Based on photographic data obtained using The UK Schmidt Telescope. The UK Schmidt Telescope was operated by the Royal Observatory Edinburgh, with funding from the UK Science and Engineering Research Council, until 1988 June, and thereafter by the Anglo-Australian Observatory. Original plate material is copyright (c) the Royal Observatory Edinburgh and the Anglo-Australian Observatory. The plates were processed into the present compressed digital form with their permission. The Digitized Sky Survey was produced at the Space Telescope Science Institute under US Government grant NAG W-2166.

completely extracted from the surrounding field based on radial position alone. In order to further enhance the cluster sequence, we defined a background CMD using the $30'' \leq R < 50''$ region and accounting for the area difference between this annulus and the central region. The background CMD was binned in 0.5 mag color-magnitude bins. We then randomly selected and subtracted stars from the cluster in equal numbers from bins matching the background CMD. The resulting CMD is shown in Figure 7. The corresponding colors for these stars are plotted as *open circles* in Figure 4.

3.1.2. Extinction to the Cluster

Most of the brightest stars in the central cluster fall along an essentially vertical track as expected for hot stars. The average color of the brightest seven of these stars is $H - K = 0.637$ which corresponds to an extinction at $2.2 \mu\text{m}$ of $A_K = 1.07$ mag ($A_V \approx 10$ mag) using the interstellar reddening curve of Mathis (1990) and an intrinsic $H - K = -0.04$ (Koornneef 1983a). Many other stars appear more reddened, typically up to $H - K \sim 2$ with some as high as 3.8. A star with $H - K = 2$ and intrinsic $H - K = 0$ would have $A_K = 3.2$ mag ($A_V \approx 32$ mag).

3.1.3. K vs. $H - K$ CMD for the ZAMS

It will be useful in discussing the W42 cluster below to have an estimate for the zero age main sequence (ZAMS) transformed into the K vs. $H - K$ plane. We have constructed such an estimate using the model results of Schaller et al. (1992). The models give bolometric luminosities (M_{bol}) and effective temperatures (T_{eff}) for stars of a given mass as they begin their evolution on the ZAMS. Using relationships for spectral type vs. T_{eff} (Vacca et al. 1996; Johnson 1966), visual bolometric correction (BC_V) vs. effective temperature (Vacca et al. 1996; Malagnini et al. 1986), $V - K$ vs. spectral type (Koornneef 1983a), and $H - K$ vs. spectral type (Koornneef 1983a), we transform the M_{bol} and T_{eff} to the K vs. $H - K$ CMD. A small correction has been made in an attempt to place the $H - K$ colors from Koornneef (1983a) onto the CIT/CTIO system. The Koornneef (1983a) colors are basically referred to the system of Johnson (1966) with newly defined colors involving H (Johnson used no H filter). In addition, Koornneef (1983b) found that interpolating an H magnitude from the observed J and K values gives a very good estimate of the observed H magnitude. Carter (1990) found no discernible color correction between the SAAO system and that of Johnson (1966). We have therefore used the transformation of Carter (1990) between the SAAO system and CIT/CTIO to transform the $H - K$ colors given by Koornneef (1983a). These corrections are at most one percent and hence negligible compared to the measurement uncertainties and scatter due to differential reddening.

The ZAMS CMD is shown in Figure 7 for a particular distance (2.2 kpc) which is discussed in §4. The values plotted in Figure 7 are listed in Table 1. These values may be compared to those

given by Hanson et al. (1997). There is generally good agreement as a function of T_{eff} . This is expected since the same models and colors were used in both cases. There are systematic differences at the $\sim \pm 0.3$ mag level for M_K as a function of spectral type since the spectral type vs. T_{eff} relation adopted here (Vacca et al. 1996; Johnson 1966) is different than that used by Hanson et al. (1997) who used the relation given by Massey et al. (1989). These differences do not affect the conclusions of §4.3 since the resulting M_K for the spectral type in question (O5–O6) is within 0.1 mag in both cases.

3.1.4. The K –band Luminosity Function

The K –band luminosity function (KLF) is shown in Figure 8. Neglecting the last five bins where the counts appear to be incomplete and the first 3 bins where the counts may be better described as uniform, the K –band counts are well fit by a power–law with index 0.4 ($\log_{10}N = 0.4 \times K + \text{constant}$).

We estimated the completeness of the KLF by performing artificial star experiments. Initially, we attempted to add stars to the original K –band image, but even adding 10% of the observed KLF resulted in recovered luminosity functions much less complete than the observed one. This is due to the high spatial density of the cluster. To avoid this problem, we constructed complete artificial frames and analyzed them in the same way as the original frame. Anticipating the result, we used the spatial density distribution of the stars on the K –band image with $K < 14$ mag (Figure 5) to generate the positions of stars on the artificial frames. The input luminosity function was constructed from two components, a uniform distribution from $8.5 \leq K \leq 10.5$, and a power–law for $10.5 < K \leq 19.5$. The total number of stars was set by the flux on the K –band image, less a uniform background component determined from the sky frame. This should be conservative regarding the number of stars since the strong nebular flux is included. This latter aspect may be balanced somewhat by the fact that the artificial frames did not include variable extinction and nebular emission. The total K –band flux in Figure 1c is 6.0 mag, not including the bright saturated star in the SE corner of the frame. The total flux of the average actual input luminosity function (Figure 9) was 5.9 mag which can be compared to the total flux in observed stars (Figure 8), $K = 6.18$ mag.

We constructed 10 artificial frames by randomly sampling the spatial distribution and luminosity functions. DoPHOT was run on each frame and the recovered stars matched to the input lists. The average recovered luminosity function, input luminosity function, and completeness fraction are shown in Figure 9. The general shape and distribution of the recovered stars in Figure 9 suggest the experiments are a fair test of completeness of the original frame. From the same input and recovered star lists, we also show the luminosity functions and completeness fraction for the stars located at $0'' \leq R < 30''$. See Figure 10.

Tests were also made to check whether somewhat steeper power–laws were also consistent

with the observed KLF. This might be the case if the crowding were sufficient to “hide” many fainter stars. Artificial star experiments analogous to those above (including the same uniform component) but with a power-law component of 0.5 are not consistent with the data. A single power-law component of this steepness produces more star light than is necessary to account for the observed total flux and produces too many stars in the recovered luminosity function at fainter magnitudes if it is required to produce approximately the correct numbers at brighter magnitudes.

3.2. Spectra

The spectra of the targets W42 #1, #2, and #3 are shown in Figure 11. The final signal-to-noise in the three spectra is typically 80–105, 75–95, and 55–78 for W42 #1, W42 #2, and W42 #3, respectively and is higher on the red end than the blue end for all three. The brightest star in the central cluster, W42 #1 ($K = 8.8$ mag), shows characteristic O star features (Hanson et al. 1996). These include C IV (2.069 μm and 2.078 μm) emission, N III (2.1155 μm) emission, Br γ (2.1661 μm) absorption, and He II (2.1891 μm) absorption. Comparison to the standards presented by Hanson et al. (1996) results in K –band spectral type of kO5–O6. These stars typically have MK spectral types of O5 to O6. The present classification system laid out by Hanson et al. (1996) does not have strong luminosity class indicators. Still, the He I (2.06 μm) and Br γ features can be used to approximately distinguish between dwarf+giants on the one hand, and supergiants on the other: the supergiants tend to have emission or weak absorption in these lines. The spectrum of W42 #1 shown in Figure 11 has been background subtracted with nearby apertures to account for the nebular emission seen in projection toward the star. The apparent absorption feature at the position of Br γ and absence of a feature at He I (2.06 μm) (which might indicate a poor subtraction of the nebular contribution), suggests that W42 #1 is a dwarf or giant star.

In contrast to W42 #1, the spectra of W42 #2 and #3 show only emission features at He I (2.06 μm) and Br γ . These spectra have also been background subtracted with nearby ($\lesssim 1.0''$) background apertures. We believe the strong emission remaining after this subtraction is related to the local environment in these stars (see §4.1).

4. DISCUSSION

The dense stellar cluster evident in Figure 1 surrounded by intense nebulosity leaves no doubt that this is a young object still emerging from its birth environment at the edge of its parent molecular cloud. The cluster appears to have emerged by clearing the foreground material to the West; darker regions with fewer stars remain toward the East. There is a suggestion of photoevaporated regions on the edge of the cloud to the East similar to those seen in M16 (Hester et al. 1996) and NGC 3603 (Brander et al. 1999). This is particularly evident in Figure 1a. This picture is consistent with the CO line maps of Lester et al. (1985), who found the peak brightness temperature of

the associated molecular cloud to be offset to the East of the W42 (G25.4SE) H II region (see their Figure 8). Higher spatial resolution images and in nebular lines are in order to further study the interaction and impact of the ionizing cluster on the molecular cloud interface.

The process of clearing the local environment is still on-going, clumps of dark material are seen in projection against the photoionized H II region (e.g. SW of the cluster center). In §3.1.2, the extinction to the brightest stars on the cluster sequence was found to be $A_K = 1.07$ mag. This value can be taken as representative of the foreground extinction to the cluster, and indicates a V magnitude of approximately 18 for W42 #1. This is consistent with the non-detection of the cluster on the DSS plates. A few stars remain after subtracting the "background" component from the CMD (§3.1.1), but these are more likely in the foreground since the extinction toward them is as low as $A_K \sim 0.3$ mag.

4.1. Young Stellar Objects

There are a host of very red objects indicated in Figures 1, 6, and 7. Such colors are suggestive of young stellar objects (YSO) in the context of an embedded stellar cluster emerging from its parent cloud. The observed colors of known populations of pre-main sequence stars (PMS) and more heavily embedded protostars appear to lie on/occupy rather well defined sequences/regions in observational color space; and their colors, which are redder than usual stellar photospheres have been successfully modeled as arising from excess emission produced by circumstellar disks (Lada & Adams 1992; Meyer et al. 1997) and envelopes (Hartmann et al. 1993; Pezzuto et al. 1997). Like normal stars, PMS objects may be seen through foreground extinction, further reddening their colors. Deeply embedded protostars may have colors with or without excess emission, but typically suffer large extinction due to the dense envelope surrounding them (Lada & Adams 1992). Obviously, protostars too may suffer additional foreground extinction.

The $J - H$ vs. $H - K$ color-color diagram is most useful in assessing whether any particular star may have excess emission. The diagram distinguishes between normal stellar colors which are seen through a column of dust, hence making them redder, and a contribution which is due to emission (reprocessed stellar light from circumstellar envelope and/or accretion luminosity from a circumstellar disk). Lada & Adams (1992) and Meyer et al. (1997) have shown that disks can provide a source of excess emission to the normal stellar colors. In Figure 4, we have plotted the classical T Tauri sequence (CTTS) from Meyer et al. (1997) along with reddening lines for the interstellar reddening law of Mathis (1990). The former locus may be understood as arising from disk luminosity and projection effects (e.g, Lada & Adams 1992 and references therein). The near infrared colors of weak lined T Tauri stars (WTTS) are similar to normal stars (Meyer et al. 1997). These stars exhibit spectra which suggest they have disks, but the disk contribution to the near infrared colors is negligible. The Herbig AeBe stars which are higher mass analogs to the CTTS show similar colors to the CTTS but extend to generally larger $H - K$ excess and with a larger contribution to the colors from circumstellar extinction (Lada & Adams 1992). The colors of these

objects have been fit by circumstellar envelope models in which the excess emission arises from reprocessed stellar light via dust heating and re-radiation (Hartmann et al. 1993; Pezzuto et al. 1997), or alternatively, from circumstellar disks with central holes (Lada & Adams 1992). We also show the reddening lines for a main sequence O star and M giant (see S3.1) which can be taken as approximate guides for the expected colors for normal stars along sight lines to the inner Galaxy. The *black squares* in Figure 4 represent all the stars in Figure 1 for which J , H , and K colors were measured. The *open circles* represent the stars in the "background subtracted" central cluster (§3.1.1).

The W42 cluster stars (including W42 #1) occupy a rather tight sequence at modest reddening in Figure 4 as expected for young massive stars seen through different columns of obscuring material. At larger reddening ($H - K$, $J - H = 1,2$), there is a larger dispersion of colors. There are also a number of stars which lie significantly beyond the reddening band for normal stars in the region of PMS stars and protostars as discussed above. Two of these objects are W42 #2 and #3. Spectra for these objects are shown in Figure 11. Neither spectrum shows stellar absorption features, though both exhibit emission at $\text{Br}\gamma$ or He I ($2.06 \mu\text{m}$) after background subtraction (§2). Accounting for the foreground extinction to W42 #1, both W42 #2 and #3 lie in a region of the color–color plot occupied by luminous protostars and Herbig AeBe stars (Lada & Adams 1992). Lada & Adams (1992) suggest that Herbig AeBe stars might be recently "uncovered" protostars given the large overlap in the color–color plot for the two objects. We believe that the position of W42 #2 and #3 in the color–color plot combined with their emission–line spectra, strongly suggests they are also luminous YSOs. The absence of absorption features is consistent with veiling due to the excess emission seen in Figure 4. In the case of W42 #2, the residual $\text{Br}\gamma$ emission may be due to a circumstellar disk; spherical or envelope distributions to the circumstellar material are also possible. Higher spectral resolution data on the $\text{Br}\gamma$ line in this object will be required to rule out models of one nature or the other. In W42 #3, the presence of He I emission but no $\text{Br}\gamma$ could be due to imperfect subtraction. W42 #3 has closer neighbors making the subtraction of the background more difficult. If the emission seen in projection toward W42 #3 is due to a compact H II region, then the He I emission may be coming from a region closer to the star than the $\text{Br}\gamma$, the latter naturally subtracting off better on these angular scales. We plan to obtain H –band spectra of W42 #2 and #3 where the excess emission should be less allowing for an improved picture of the nature of the embedded objects which give rise to the emission spectra seen at K .

There are several other stars with similar or slightly lower brightness indicated in Figure 7, but with apparently normal colors for hot stars. This suggests a mixture of massive objects with and without circumstellar (possibly disk) signatures as seen in M17 (Hanson et al. 1997). Like M17, the YSOs indicate a very young age for the cluster.

The situation in W42 may be compared to other stellar clusters in giant H II regions. For M17, Lada et al. (1991) report that the vast majority of cluster stars they studied have infrared excesses. This result should be confirmed with higher spatial resolution images; the photometry presented by Lada et al. (1991) was performed by summing the flux in $4.8''$ diameter apertures on

their $0.8'' \text{ pix}^{-1}$ images. Lada et al. (1991) note that their data set was analyzed with profile fitting by Gatley, et al. (1991) who obtain similar results, and Hanson et al. (1997) clearly show that at least some of the massive stars in M17 have disk-like spectroscopic features. Gatley, et al. (1991) find far fewer stars with excess emission in the Orion Trapezium cluster and attribute this to a mixture of older and younger stars. However, Zinnecker et al. (1993) reach a different conclusion regarding the ages of the Orion cluster stars, and we will discuss this further in the next section. In W43 (Paper I), only a handful of objects appear in the excess emission region of the color–color plot and none of the three spectroscopically classified hot stars do. The brightest object in W43 exhibits Wolf–Rayet features in its K –band spectrum suggesting an older age relative to W42. This is similar to NGC 3603, R136, and the Arches (see the discussion in Paper I and references therein), and the implication is that while such stars may still be core hydrogen burning, they are not on the ZAMS.

These comparisons need to account for the fact that the extinction is generally greater in W42 and (much so) in W43, so that many objects are not detected at J or H and hence do not appear in the color–color plot. Clearly, high spatial resolution, homogeneous data sets, each analyzed in detail for completeness at J , H , and K would be useful in assessing the intrinsic fractions of stars with excess emission in embedded clusters in giant H II regions.

Without spectra, it is not possible to identify the nature of the remaining objects in the color excess region of Figure 4, though in the context of this young cluster, it is likely that some are PMS stars or protostars. It is also clear from Figure 4 that some YSOs can occupy the same region of color space as normal stars. Some of the cluster stars in Figure 4 near $(H - K, J - H = 1, 2)$ where the dispersion in color is larger might be a combination of WTTS with essentially normal stellar colors and CTTS/Herbig AeBe stars with smaller excess emission, the actual nature depending also on the luminosity of any particular object. Alternately, these could be normal main sequence stars. Finally, some could be normal K or M giants in the background, though it is unlikely that many are, given the large number of stars in close association with the central region of the cluster and the fact that we have subtracted a background component from the CMD.

Inspection of Figures 3 and 4 indicates that W42 #3 has varied in brightness and color between the 1998 and 1999 observations presented here, becoming fainter at K and redder. Color and brightness variations in YSOs can be explained by a combination of changes in the accretion luminosity produced by the circumstellar disk and changes in the extinction toward the source. Skrutskie et al. (1996) monitored a sample of YSOs for color changes, finding the slopes of the colors (measured over day to year timescales) in the $J - H$ vs. $H - K$ color–color diagram were intermediate between the CTTS locus (excess color arising from disk luminosity) and pure variations along the interstellar reddening lines such as might occur when clumps of obscuring material pass in front of the line of sight to the YSO. Skrutskie et al. (1996) found some YSO variations were consistent with one or the other effect dominating. The color variation for W42 #3 appears most consistent with a change in the local extinction.

4.2. The K –band Luminosity Function

The KLF has been used as the basis for mass function determinations in young embedded or obscured massive star clusters. Lada et al. (1991) found that the M17 cluster KLF had a slope consistent with the Salpeter (1955) initial mass function (IMF) value if the M17 stars were normal main sequence type, but noting that this was difficult to reconcile with their finding that essentially all the M17 cluster stars had infrared excesses. Only in the case where such excesses arise in passive disks could their mass function determination still follow from the KLF. Gatley, et al. (1991) present a KLF for the Trapezium cluster in Orion (M42). They found the slope of the KLF to be inconsistent with that for the Salpeter (1955) initial mass function (IMF), hypothesizing that there are substantial numbers of older stars in M42 as well as very young ones. However, Zinnecker et al. (1993) found that the KLF in M42 was consistent with a population of only very young stars if PMS evolutionary tracks were used instead of assuming the cluster stars were on the main sequence. Zinnecker et al. (1993) show that deuterium burning on the PMS can cause peaks in the KLF which are a function of age thus producing luminosity functions different from expected if main sequence mass–luminosity relations are assumed. More recently, the detailed optical imaging/spectroscopic investigation of Hillenbrand (1997) exquisitely details the young main sequence and PMS stellar population in the Orion Trapezium cluster, clearly demonstrating the overall youth of the cluster.

Figer et al. (1999b) presented a mass function determination for the Arches cluster located near the Galactic center (GC). They find that the Arches cluster may have upwards of 100 O stars and an age of ~ 2 Myr. Using their observed KLF and a mean value for A_K , these authors determined the mass function by relating the K magnitudes to stellar mass using the Meynet et al. (1994) stellar evolutionary models. Figer et al. (1999b) find a mass function in the Arches which is significantly flatter than Salpeter (1955). They attribute this result to the different pre-conditions for star formation in the central few hundred parsecs of the Galaxy which they argue should favor higher mass stars. This is in contrast to the situation elsewhere in the Galaxy and in the Large Magellanic Cloud (LMC) (Massey & Hunter 1998). Massey & Hunter (1998) find from a combination of spectroscopy and imaging that the IMF is similar for OB associations and dense massive star clusters (most notably R136 in the LMC) and in agreement with a Salpeter (1955) IMF.

The preceding discussion indicates that care must be taken in transforming the KLF into a mass function, including the effects of PMS evolution. In this sense, the determination of a mass function for W42 is premature given the implied young age and lack of transformations between PMS models and near infrared colors (which should include the effects of associated disk emission). However, a comparison to the different KLFs is warranted.

In §3.1 we derived the KLF for the inner $30''$ central cluster in W42 and showed that it should be complete to $\gtrsim 80\%$ for $K \leq 15$ mag. The measured slope of the cumulative counts in the central $30''$ KLF ($K \leq 15$, correcting for incompleteness) is 0.38 ± 0.016 . If we consider only stars in the background subtracted CMD (Figure 7, the measured slope ($K \leq 15$) is 0.36 ± 0.011 . The slope in

our background annulus ($30''$ to $50''$, $K \leq 15$, correcting for incompleteness) is 0.51 ± 0.017 . These values may be compared to the results of Lada et al. (1991), Zinnecker et al. (1993), and Figer et al. (1999b). For convenience, we compare the power-law slope to the *cumulative* KLF which Lada et al. (1991) also calculated for their data. In M17, Lada et al. (1991) report a slope of 0.26, which they claim is consistent with the Salpeter (1955) IMF. We have calculated approximate slopes for Zinnecker et al. (1993) and Figer et al. (1999b) from figures of the published luminosity functions; these are 0.39 ± 0.016 and 0.28 ± 0.013 , respectively. Figer et al. (1999b) conducted completeness detailed tests and corrected the published counts. Lada et al. (1991) conducted more rudimentary checks on completeness and report the KLF for the magnitude range they believe to be complete. Zinnecker et al. (1993) and Gatley, et al. (1991) conducted no completeness tests using artificial stars, to the best of our knowledge, though Zinnecker et al. (1993) claim the KLF is complete. All the KLFs discussed here are defined for the central clusters in the respective star forming regions, and none have been corrected for reddening. Thus our comparison is only for the slopes of the KLFs and does not account for possible differences resulting from differential reddening.

The KLF in W42 appears to be more similar to that in Orion (i.e. relatively steep) than in M17 or the Arches. Given the likely presence of YSOs as discussed above, we may be seeing the effects of PMS evolution on the number counts as is the case for the Trapezium. Both the Arches and M17 clusters clearly have more massive stars than are present in the central cluster of W42 or the Trapezium (Cotera et al. 1996; Hanson et al. 1997). The apparent KLFs in these latter two clusters appear at least superficially similar, though Figer et al. (1999b) and Lada et al. (1991) reach rather different conclusions when converting to mass functions. Figer et al. (1999b) derive an IMF which is much flatter (\sim factor of 2) than Salpeter (1955), while Lada et al. (1991) find a mass function which is possibly consistent with Salpeter (1955).

4.3. Distance

In §3.2 we classified the spectrum of the bright central star, W42 #1, as an early to mid O type (\approx O5–O6). Several lines of evidence presented above suggest that the W42 cluster is quite young. If we take W42 #1 to be on the ZAMS then its apparent brightness would give a distance to the cluster of 2.2 kpc, considerably closer than the radio distance (3.7 kpc, see §3). In §3.2, we argued that the spectrum of W42 #1 was most similar to those for the dwarf or giant luminosity classes. Using the average M_V from Vacca et al. (1996) for dwarf stars and colors from §3, gives 2600_{700}^{1000} kpc. If the giant star M_V from Vacca et al. (1996) is used, then the distance estimate becomes 3400_{900}^{1200} pc. The uncertainty in the distance estimate is completely dominated by the luminosity class assumed and the scatter in the intrinsic M_V of O stars (± 0.67 mag). The uncertainties in the reddening and apparent magnitude are negligible in comparison: a few percent for m_K and $\lesssim 10\%$ for A_K , where the largest part of the uncertainty is in the choice of reddening law (see Mathis 1990). These distance estimates are in agreement with Lester et al. (1985) who argued that W42 (G25.4SE) was at the near distance given by the radio recombination line velocity and Galactic

rotation model. Depending on the true luminosity of W42 #1, the cluster may even be somewhat closer. Smith et al. (1978) estimated the Lyc luminosity of W42 to be $8.2 \times 10^{50} \text{ s}^{-1}$ assuming the far kinematic distance (13.4 kpc). Adopting the ZAMS distance (2.2 kpc) as indicated by the young nature of the cluster (stars W42 #2 and #3) considerably reduces the expected ionizing flux to $2 \times 10^{49} \text{ s}^{-1}$.

In Figure 7, we have plotted a zero age main sequence (ZAMS) derived from the models of Schaller et al. (1992) ($Z = 0.02$); see §3.1.3. We have placed the ZAMS in Figure 7 at 2200 pc, assuming that the W42 #1 is on the ZAMS. In this case, the (incomplete) cluster sequence reaches early K type stars. For the Trapezium (Zinnecker et al. 1993) claim that the KLF shows an intrinsic peak well above the sensitivity of their K –band images. This peak is due to the PMS evolution of the lower mass stars and is sensitive to age on the PMS. For the close distance to W42 implied if W42 #1 is on the ZAMS, the similarity found above for the KLF of W42 compared to the Trapezium then suggests a similar effect on the KLF may be at work. I.e., the fainter magnitudes may correspond to lower mass PMS stars. In the present case, we are not claiming to see a real turn over in the KLF (as Zinnecker et al. do in Orion) since this occurs where the K –band counts are demonstrably incomplete due to crowding.

For a distance of 2.2 kpc, the cluster has a radius of 0.32 pc at $30''$. The surface density in the inner $10''$ (Figure 5) is then within a factor of two for that in the Trapezium (McCaughrean & Stauffer 1994, $\sim 6500 \text{ pc}^{-2}$) not accounting for the substantial incompleteness in the present case. W42 is thus quite dense, and this is another indication of its young age (McCaughrean & Stauffer 1994; Figer et al. 1999b).

The ZAMS clearly demonstrates the lack of any sensitivity to temperature in the hot stars at near infrared wavelengths. This means that traditional methods of cluster fitting (in the observational color–magnitude plane) for age or distance can not be used and only through suitable numbers of infrared spectra (resulting in M_{bol} and T_{eff}) will the cluster properties truly emerge. The lack of temperature sensitivity in the near infrared colors does, however, lead to accurate estimates of the foreground extinction.

5. SUMMARY

We have presented high spatial resolution J , H , and K images of the massive star cluster at the heart of the giant H II region W42. Our K –band spectra of three of the brightest four stars in the central $30''$ of the cluster indicate a very young population. The brightest star W42 #1 is classified as kO5–O6 based on the system of Hanson et al. (1997). Such stars are typically associated with MK O5–O6.5 dwarfs. W42 #2 and W42 #3 show no stellar absorption features. This fact, combined with their position in the excess emission band of the $J - H$ vs. $H - K$ color–color plot, leads us to classify them as YSOs.

The KLF was computed and compared to other massive star clusters. The KLF in W42

appears more similar to that of the Trapezium than to the more massive clusters in M17 and the Arches. The steepness of the KLF in the Trapezium has been attributed to the PMS stars present there, and it is possible that a similar effect is present in W42 given our spectroscopic and imaging evidence for YSOs.

Our spectrum of W42 #1 confirms the results of Lester et al. (1985) that W42 (G25.4SE) can not be at the far kinematic distance. Earlier estimates of the Lyc output from this giant H II region must therefore be revised downward (by \sim an order of magnitude). If W42 #1 is on the ZAMS, as we argue based on the presence of young stellar objects, then the cluster is even closer than the near kinematic distance (3.7 kpc). We estimate 2.2 kpc. In this case, W42 should not be considered a giant H II region as defined in §1. Our spectrum of W42 #1 is not sensitive to luminosity class, though it suggests a dwarf or giant classification.

PSC appreciates continuing support from the National Science Foundation. We wish to acknowledge the continuing excellent support received from the CTIO mountain staff, particularly from night assistants Hernán Tirado, Patricio Ugarte, and Alberto Zuñiga.

REFERENCES

Blum, R.D., Ramond, T.M., Conti, P.S., Figer, D.F., & Sellgren, K. 1997, AJ, 113, 1855

Blum, R.D., Damineli, A., & Conti, P.S. 1999, AJ, 117, 1392 (Paper I)

Brander, W., et al. 1999, BAAS, 194.6808B

Carter, B. S. 1990, MNRAS, 242, 1

Cotera, A., Erickson, E. F., Colgan, S. W. J., Simpson, J. P., Allen, D. A., & Burton M. 1996, ApJ, 461, 750

DePoy, D. L., Atwood, B., Byard, P., Frogel, J. A., & O'Brien, T. 1993, in SPIE 1946, "Infrared Detectors and Instrumentation," pg 667

Elias, J. H., Frogel, J. A., Matthews, K., & Neugebauer, G. 1982, AJ, 87, 1029

Figer, D. F., McLean, I. S., & Najarro, F. 1997, ApJ, 486, 420

Figer, D. F., McLean, I. S., & Morris, M. 1999, ApJ, 506, 384

Figer, D. F., Kim, S. S., Morris, M., Serabyn, E., Rich, R. M., McLean, I. S., 1999, ApJ, in press

Frogel, J. A., Persson, S. E., Matthews, K., & Aaronson, M. 1978, ApJ, 220, 75

Gatley, I., Merrill, K. M., Fowler, A. M., & Tamura, M. 1991, in Astrophysics with Infrared Arrays, ed. R. Elston, ASP Conf. Ser. 14, p230

Hanson, M. M., Conti, P. S., & Rieke, M. J. 1996, *ApJS*, 107 281

Hanson, M. M., Howarth, I.D., & Conti, P.S. 1997, *ApJ*, 489, 698

Hanson, M. M., Rieke, G., & Luhman K. L. 1998, *AJ*, 116 1915

Hartmann, L., Kenyon, S. J., & Cavalet, N. 1993, *ApJ*, 407, 219

Hester, J. J., et al. 1996, *AJ*, 111, 2349

Hillenbrand, L. A. 1997, *AJ*, 113, 1733

Johnson, H. 1966, *ARA&A*, 4, 193

Koornneef, J. 1983, *A&AS*, 51, 489

Koornneef, J. 1983, *A&A*, 128, 84

Lada, C. J., DePoy, D. L., Merrill, K. M., & Gatley, I. 1991, *ApJ*, 374, 533

Lada, C. J. & Adams F. C. 1992, *ApJ*, 393, 278

Lester, D.F., Dinerstein, H.L., Werner, M.W., Harvey, P.M., Evans II, N.J., & Brown, R.L. 1985, *ApJ*, 296, 565

Malagnini, M. L., Morossi, C., Rossi, L., & Kurucz, R. L. 1986, *A&A*, 162, 140

Massey, P., Parker, J., & Garmany, C. D. 1989, *AJ*, 98, 1305

Massey, P., Johnson, K., & DeGioia-Eastwood, K. 1995, *ApJ*, 454, 151

Massey, P. & Hunter, D. A. 1998, *ApJ*, 493, 180

Mathis, J.S. 1990, *ARA&A*, 28, 37

McCaughrean, M. J. & Stauffer, J. R. 1994, *AJ*, 108, 1382

Meyer, M. R., Calvet, N., & Hillenbrand, L. A. 1997, *AJ*, 114, 288

Meynet G., Maeder A., Schaller G., Schaerer D., Charbonnel C. 1994, *A&A*, 103 97

Morris, M. & Serabyn, E. 1996, *ARA&A*, 34, 645

Olivia, E. & Origlia, L. 1992, *A&A*, 254, 466

Pérez, G. & Elston, R. 1998, *Proc. SPIE*, 3352, 328

Persson, S. E., Murphy, D. C., Krzeminski, W., & Roth, M. 1998, *AJ*, 116, 2475

Pezzuto, S., Strafella, F., Lorenzetti, D. 1997, *ApJ*, 485, 290

Salpeter, E. E. 1955, *ApJ*, 121, 161

Schaller G., Schaefer D., Meynet G., Maeder A., 1992, *A&AS*, 96, 269

Schechter, P. L., Mateo, M. L., & Saha, A. 1993, *PASP*, 105, 1342

Skrutskie, M. F., Meyer, M. R., Whalen, D., & Hamilton C. 1996, *AJ*, 112, 2168

Smith, L.F., Biermann, P. & Mezger, P.G. 1978, *A&A*, 66, 65

Vacca, W. D., Garmany, C. D., & Shull, J. M. 1996, *ApJ*, 460, 914

Zinnecker, H., McCaughrean, M. J., & Wilking, B. A. 1993, in *Protostars and Planets III*, eds E. Levy & J. Lunine, (Tucson: University of Arizona Press), p429

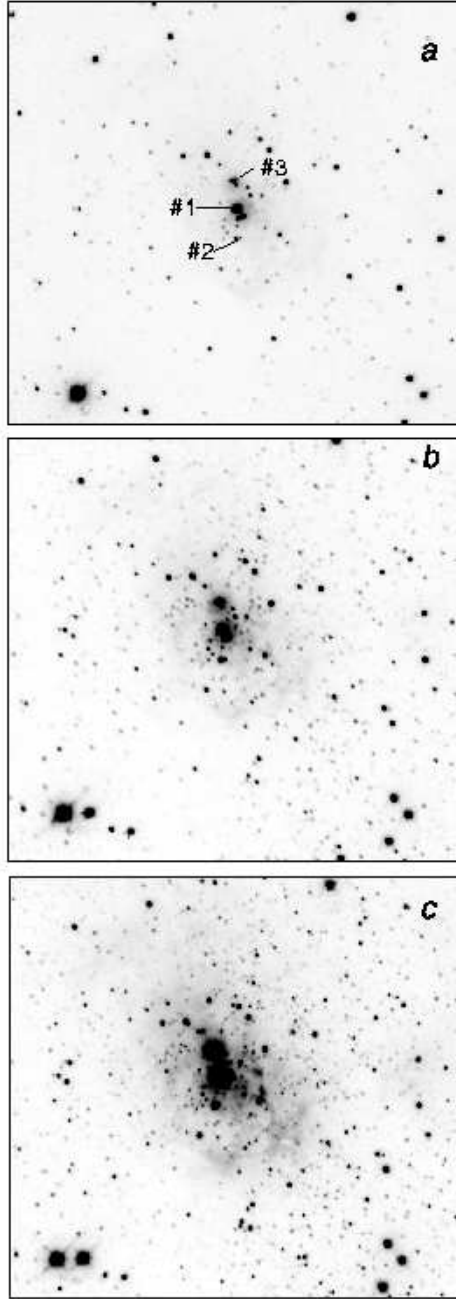


Fig. 1.— JHK images of the massive star cluster in W42. North is up, East to the left, and the scale is $0.16''$ pix^{-1} in these $\sim 1.8' \times 1.7'$ images. The combined images have point sources with FWHM of approximately $0.6''$, $0.7''$, and $0.6''$ at J , H , and K , respectively. a) J –band. b) H –band. c) K –band. Stars with spectra presented in Figure 11 are labeled in a. W42 #3 is not the most prominent source at J (but is at K) near the line marking its position. See also Figure 2.



Fig. 2.— False color image (K = red, H = green, J = blue) constructed from the images shown in Figure 1. North is up, East to the left.

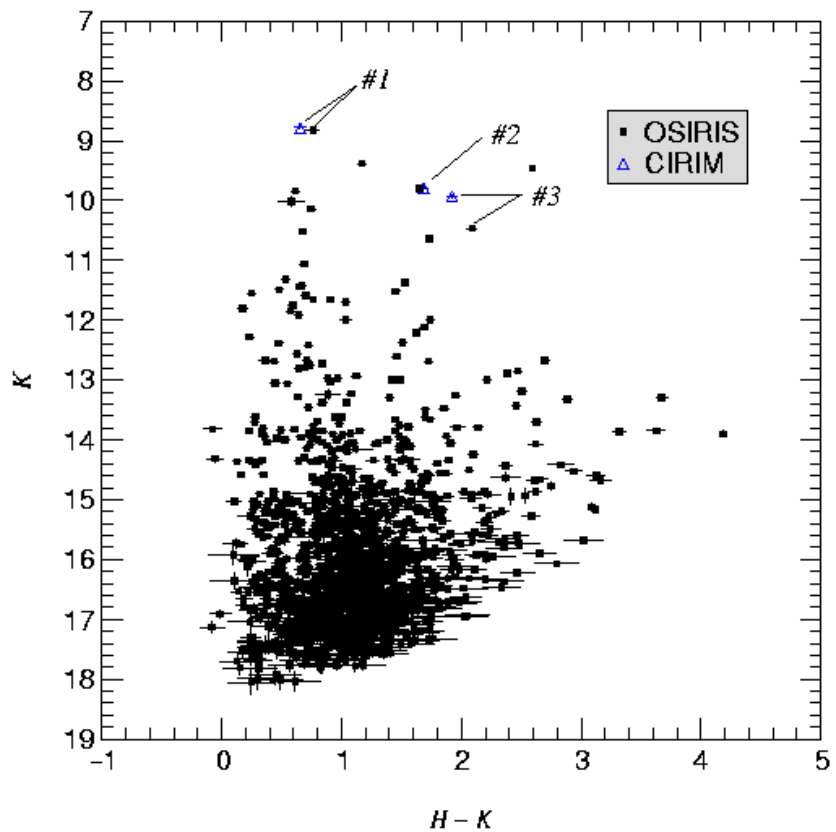


Fig. 3.— $H - K$ color-magnitude diagram (CMD) for the W42 cluster and surrounding field. Stars for which spectra are presented are labeled. The *open triangles* are from the CIRIM data and are plotted for stars brighter than the OSIRIS saturation limit where possible (the CIRIM field of view is smaller than that for OSIRIS).

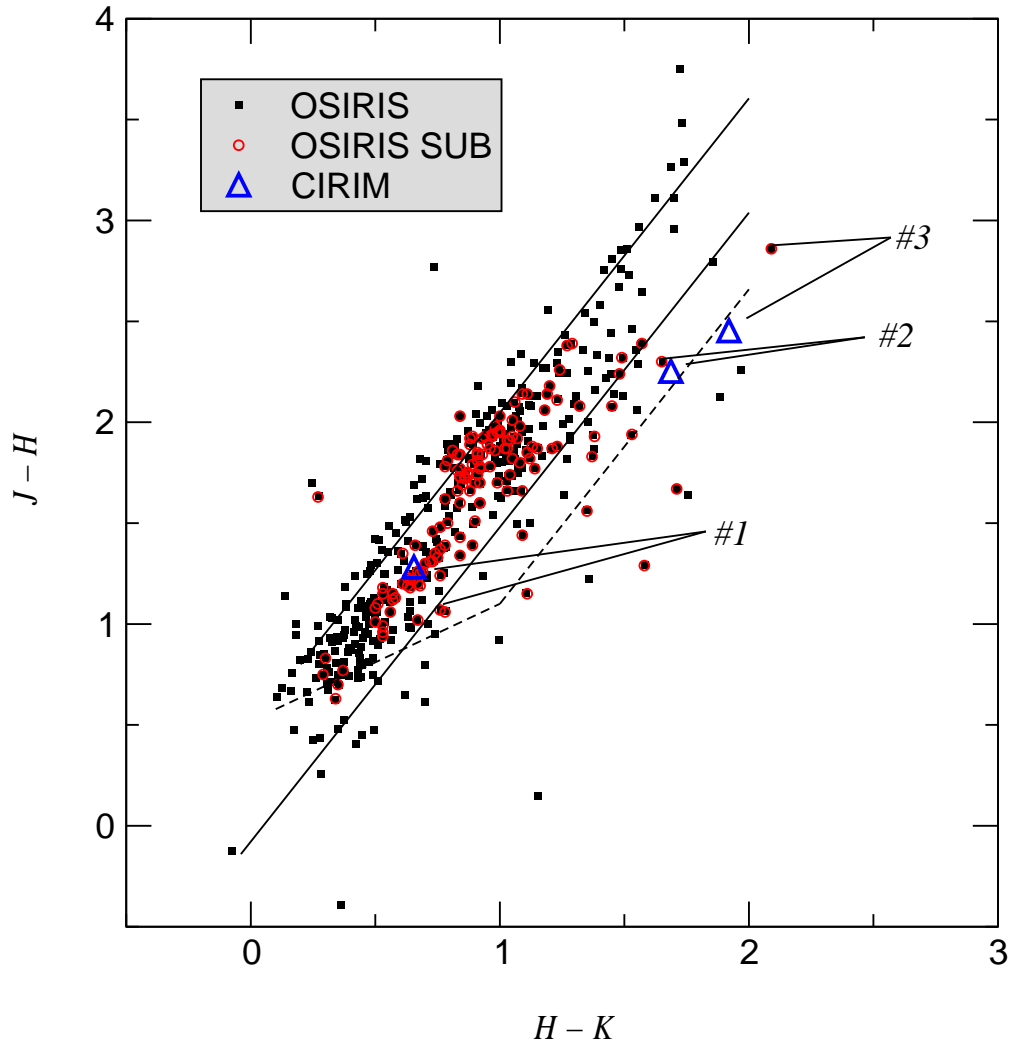


Fig. 4.— $J-H$ vs. $H-K$ color–color diagram for the the W42 cluster. All stars in the field detected at J , H , and K are plotted as *filled black squares*. Stars in the final statistically subtracted central cluster are plotted as *open circles*. The CIRIM data for W42 #1, #2, and #3 are also presented (*open triangles*). For comparison, the reddening lines for early O stars (lower line, $H-K = -0.04$, $J-H = -0.14$, (Koornneef 1983a); see text) and M giants (upper line, $H-K = 0.2$, $J-H = 0.8$, (Frogel et al. 1978)) are shown. The classical T Tauri star locus (Meyer et al. 1997) is also shown for reference (*dashed line*). W42 #3 appears to have varied significantly in both colors; see text.

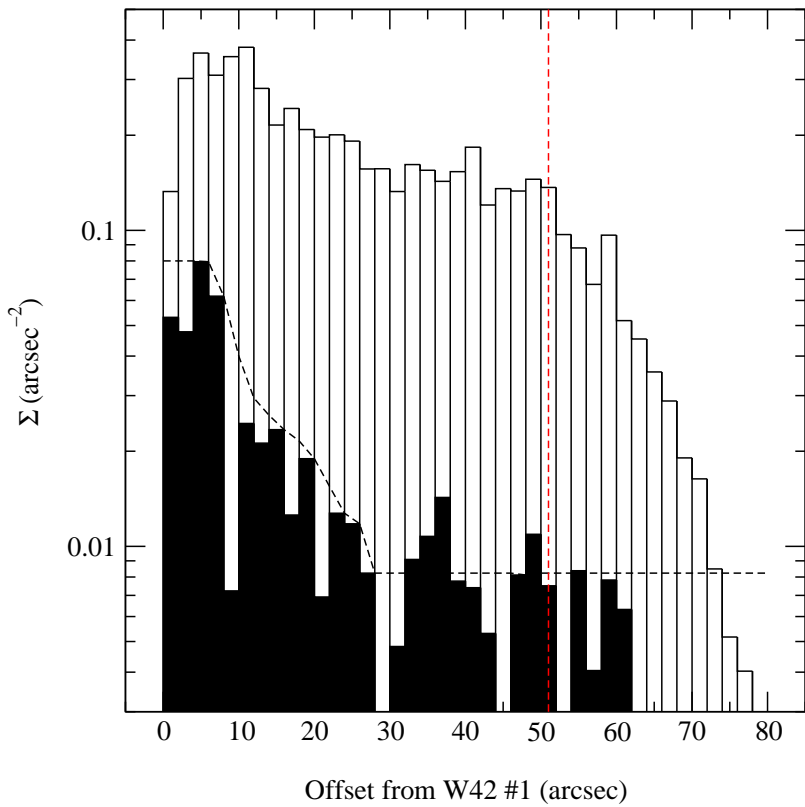


Fig. 5.— The observed K –band radial surface density. Radius is defined as distance in arcsec from the bright central star W42 #1. A central cluster can be defined at $R < 30''$ where the counts become uniform. The *dashed vertical line* represents the array edge where the radial counts begin to fall as expected due to the rectangular shape of the field. The *solid histogram* is for stars with $K \leq 14$ mag where the number counts are nearly complete, and the curve represents the radial surface density distribution used in the artificial star experiments to gauge completeness; see text.

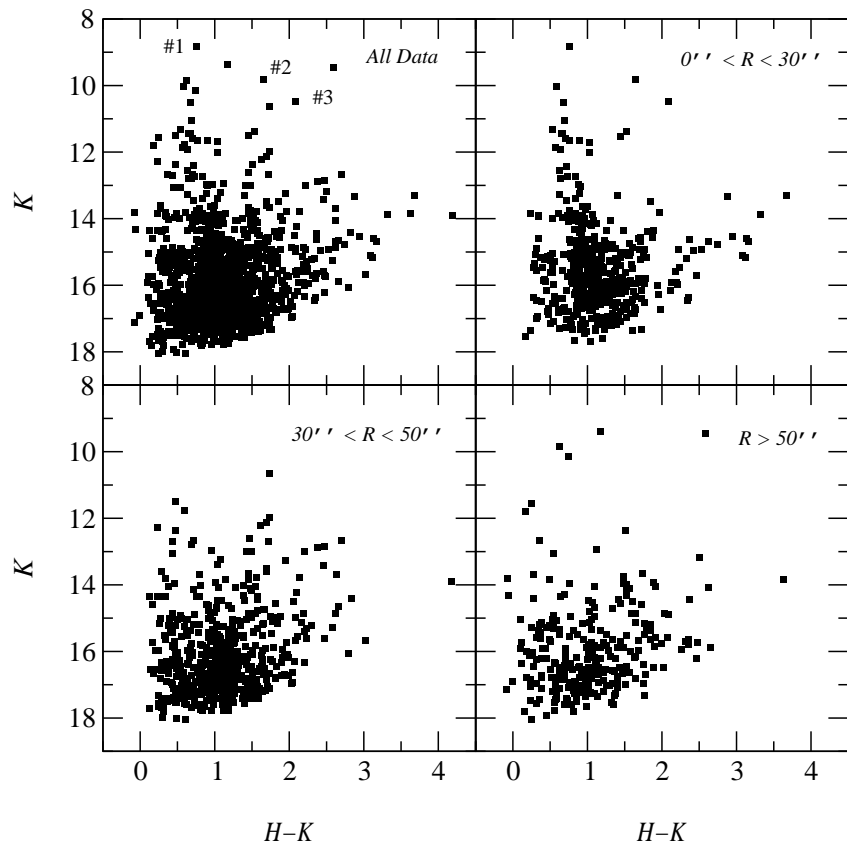


Fig. 6.— The $H - K$ color-magnitude diagram as a function of radial position. By selecting stars at $R < 30''$ as indicated in Figure 5, the central cluster sequence becomes more well defined relative to the background.

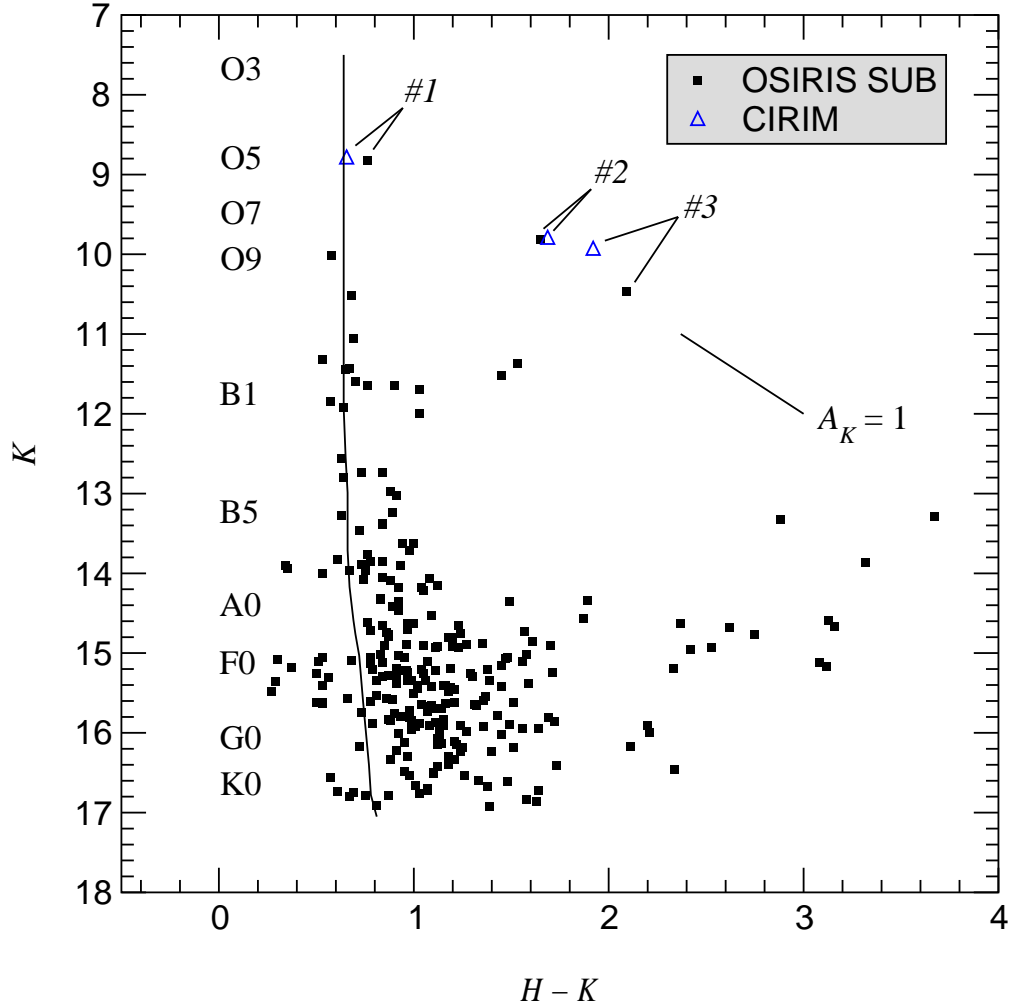


Fig. 7.— $H - K$ vs. K color-magnitude diagram (CMD) for the central cluster. A background component has been subtracted based on the number and position of stars in the $30'' < R < 50''$ CMD shown in Figure 6; see text. The *solid line* shows the relationship for the ZAMS based on the $Z = 0.02$, high mass-loss models of Schaller et al. (1992); see Table 1. The transformation to the observational plane is discussed in the text. CIRIM data (*open triangles*) are also shown for W42 #1, W42 #2, and W42 #3; see Figure 3.

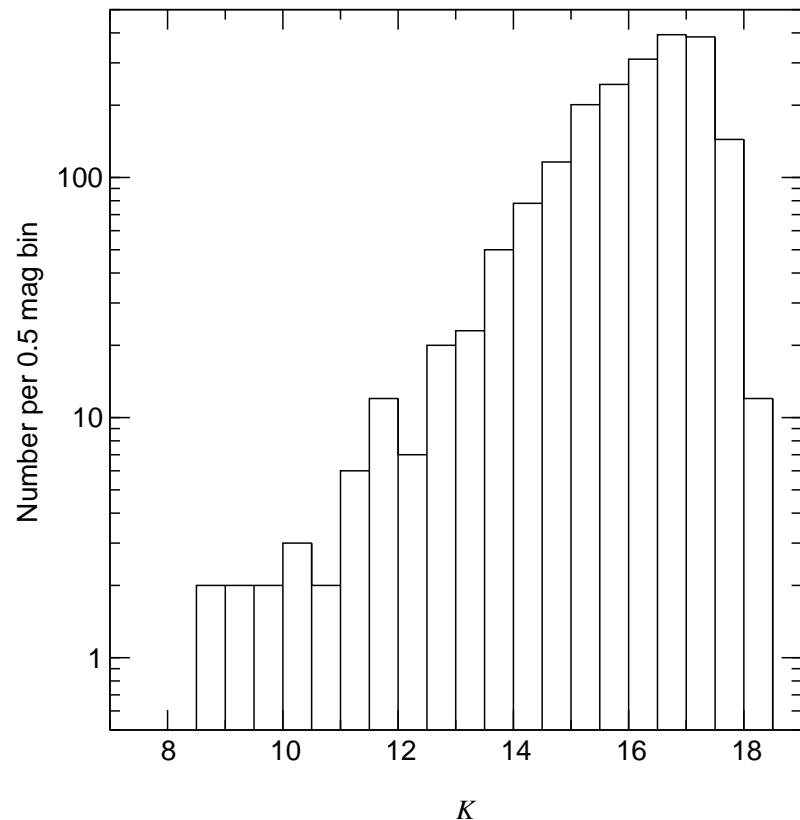


Fig. 8.— The observed K –band luminosity function (KLF) for the entire area shown in Figure 1c. No corrections for extinction or completeness have been made.

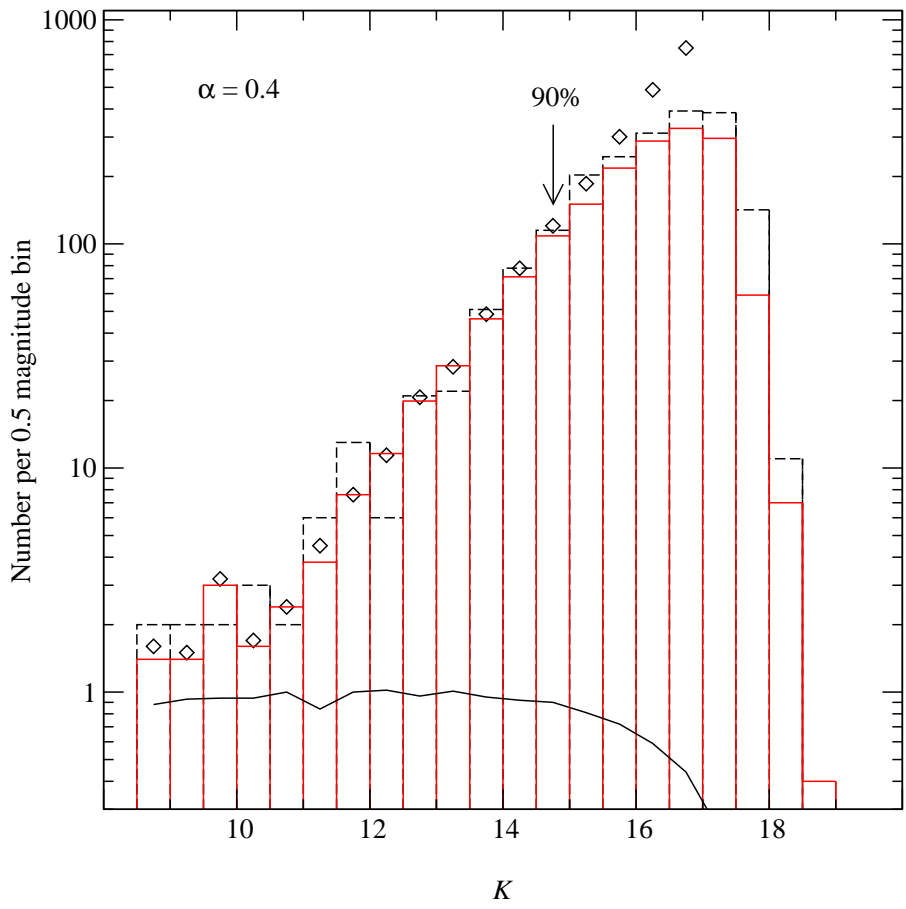


Fig. 9.— Artificial luminosity functions and the K –band completeness limit. The input (*open diamonds*) luminosity function and recovered (*solid histogram*) luminosity function are shown for an average of 10 artificial frames. For comparison, the observed K -band luminosity function is also plotted. The input luminosity function consists of a uniform distribution for the brightest stars and a power–law with index 0.4 for the remainder; see text for details. The (*solid line*) is a ratio of the recovered to input luminosity functions.

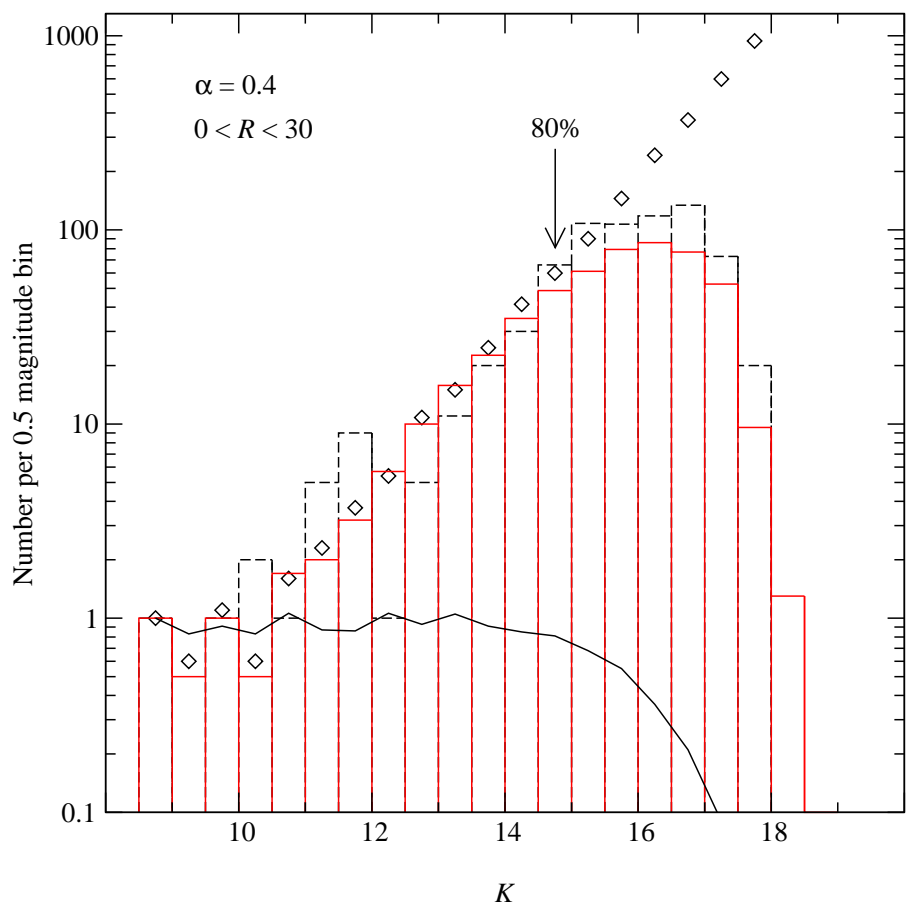


Fig. 10.— Same as Figure 9 but for stars located in the central $30''$ of the cluster.

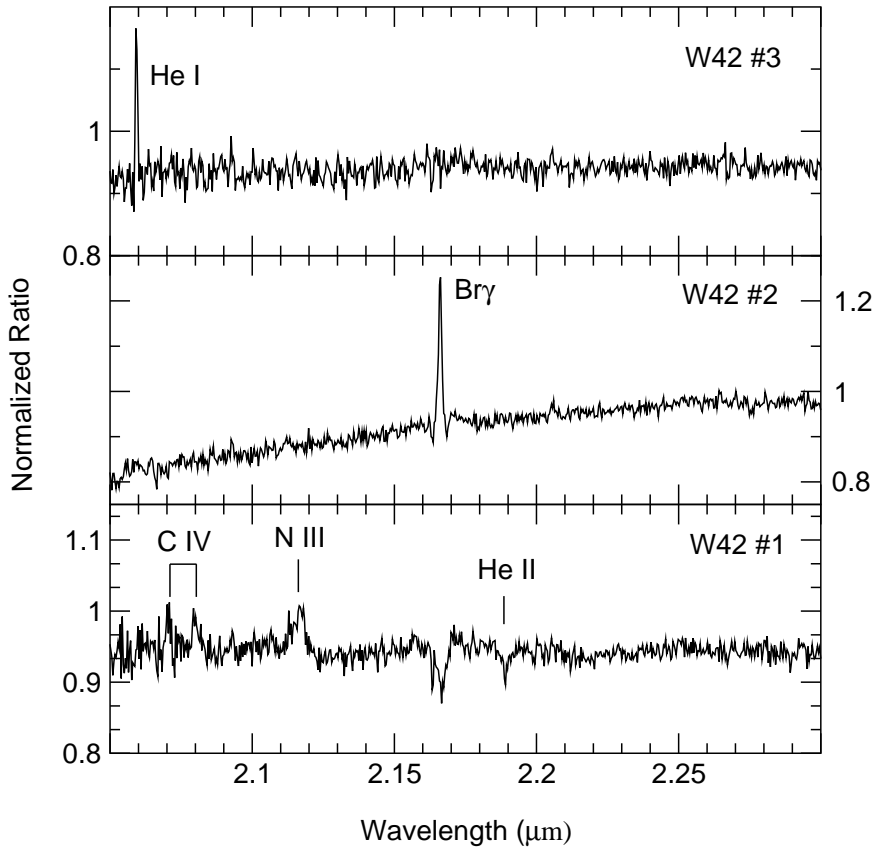


Fig. 11.— K –band spectra for three of the brightest stars in the W42 cluster. The two pixel resolution is $\lambda/\Delta\lambda \approx 3000$. The spectra were summed in apertures $0.64''$ wide \times a slit width of $0.48''$ and include background subtraction from apertures centered $\lesssim 1.0''$ on either side of the object.

Table 1. ZAMS Properties

SpType	$T_{\text{eff}}^{\text{a}}$	Mass ^b	$M_{\text{bol}}^{\text{b}}$	M_V^{c}	M_K	$V - K^{\text{d}}$	$H - K^{\text{d}}$
O3	51230	89.7	-10.28	-5.73	-4.80	-0.93	-0.05
O4	48670	65.1	-9.74	-5.34	-4.41	-0.93	-0.05
O4.5	47400	56.4	-9.50	-5.17	-4.24	-0.93	-0.05
O5	46120	49.3	-9.24	-5.00	-4.07	-0.93	-0.05
O5.5	44840	43.6	-8.97	-4.82	-3.89	-0.93	-0.05
O6	43560	38.9	-8.70	-4.62	-3.69	-0.93	-0.05
O6.5	42280	34.9	-8.41	-4.43	-3.50	-0.93	-0.05
O7	41010	31.5	-8.12	-4.23	-3.30	-0.93	-0.05
O7.5	39730	28.6	-7.84	-4.04	-3.11	-0.93	-0.05
O8	38450	26.0	-7.55	-3.85	-2.92	-0.93	-0.05
O8.5	37170	23.7	-7.28	-3.68	-2.75	-0.93	-0.05
O9	35900	21.6	-7.01	-3.51	-2.62	-0.89	-0.05
O9.5	34620	19.7	-6.75	-3.36	-2.49	-0.87	-0.05
B0	33340	17.9	-6.49	-3.21	-2.36	-0.85	-0.05
B0.5	32060	16.3	-6.23	-3.07	-2.28	-0.79	-0.04
B1	21500	7.2	-3.52	-1.70	-0.94	-0.76	-0.04
B2	18000	5.4	-2.31	-0.92	-0.25	-0.67	-0.04
B3	15500	4.3	-1.39	-0.36	0.21	-0.57	-0.03
B5	13800	3.6	-0.74	0.09	0.52	-0.43	-0.02
B7	12200	3.0	-0.07	0.59	0.89	-0.30	-0.02
B9	10600	2.5	0.70	1.15	1.29	-0.14	-0.01
A0	9850	2.2	1.13	1.44	1.44	0.00	0.00
A2	9120	2.0	1.59	1.76	1.63	0.13	0.01
A5	8260	1.8	2.23	2.15	1.80	0.35	0.02
A7	7880	1.7	2.55	2.42	1.97	0.45	0.02
F0	7030	1.4	3.36	3.23	2.44	0.79	0.04
F2	6700	1.3	3.72	3.61	2.68	0.93	0.05
F5	6400	1.2	4.07	3.98	2.97	1.01	0.06
F8	6000	1.1	4.58	4.52	3.40	1.12	0.06
G0	5900	1.1	4.71	4.67	3.45	1.22	0.07
G2	5770	1.1	4.89	4.86	3.46	1.40	0.08
G5	5660	1.0	5.05	5.04	3.49	1.55	0.08
G8	5440	1.0	5.37	5.41	3.81	1.60	0.09

Table 1—Continued

SpType	$T_{\text{eff}}^{\text{a}}$	Mass ^b	$M_{\text{bol}}^{\text{b}}$	M_V^{c}	M_K	$V - K^{\text{d}}$	$H - K^{\text{d}}$
K0	5240	0.9	5.69	5.76	4.01	1.75	0.10
K2	4960	0.8	6.15	6.30	4.05	2.25	0.13

^a T_{eff} vs. SpType from Vacca et al. (1996) and Johnson (1966)

^bDetermined from T_{eff} and models of Schaller et al. (1992)

^cDetermined from T_{eff} and bolometric correction relation given by Vacca et al. (1996, $T_{\text{eff}} > 28000$) and Malagnini et al. (1986, $T_{\text{eff}} \leq 28000$)

^dKooreneef (1983), corrected to the CIT/CTIO system; see text